U.S. DEPARTMENT OF ENERGY | Office of Science

DOE/SC-ARM-TR-329

North Slope of Alaska XSAPR b1 Data Processing Report: April 2024-April 2025

M Rocque
Y-C Feng
M Deng
A Theisen
E Schuman
A Matthews
I Lindenmaier

February 2026

ARM

DISCLAIMER

North Slope of Alaska XSAPR b1 Data Processing Report: April 2024-April 2025

M Rocque, Pacific Northwest National Laboratory (PNNL)
E Schuman, PNNL
Y-C Feng, PNNL
A Matthews, PNNL
M Deng, PNNL
I Lindenmaier, PNNL
A Theisen, Argonne National Laboratory

February 2026

How to cite this document:

Rocque, M, E Schuman, Y-C Feng, A Matthews, M Deng, I Lindenmaier, and A Theisen. 2026. North Slope of Alaska XSAPR b1 Data Processing Report: April 2024-April 2025. U.S. Department of Energy, Atmospheric Radiation Measurement User Facility, Richland, Washington. DOE/SC-ARM-TR-329.

Work supported by the U.S. Department of Energy,
Office of Science, Office of Biological and Environmental Research

Acronyms and Abbreviations

2D	two-dimensional
ARM	Atmospheric Radiation Measurement
BARC	Barrow Arctic Research Center
CMAC	Corrected Moments in Antenna Coordinates Value-Added Product
CSU	Colorado State University
DOE	U.S. Department of Energy
GE	general sensitivity
HSRHI	hemispheric range height indicator
KAZR	Ka-band ARM Zenith Radar
KDP	specific differential phase
LPM	laser precipitation monitor
NCP	normalized coherent power
NSA	North Slope of Alaska
PNNL	Pacific Northwest National Laboratory
PPI	plan position indicator
RHI	range height indicator
SAIL	Surface Atmosphere Integrated Field Laboratory
SNR	signal-to-noise ratio
SQI	signal quality index
UTC	Coordinated Universal Time
VAP	value-added product
VPT	vertically pointing scan
wv	water vapor
XSAPR	X-band Scanning ARM Precipitation Radar
ZDR	differential reflectivity

Contents

Figures

Tables

1.0 Introduction

The North Slope of Alaska (NSA) atmospheric observatory, operated by the U.S. Department of Energy (DOE)'s Atmospheric Radiation Measurement (ARM) User Facility, is a measurement site in the Arctic that has been collecting crucial atmospheric data for more than 25 years. The central facility located in Utqiaġvik, Alaska (formerly known as Barrow) hosts a suite of instruments that are used to better understand arctic processes, which are often not well represented in earth system models. The NSA site sits only a few kilometers from the Arctic Ocean, which also makes it a prime location to study complex ocean-atmosphere-ice interactions. Arctic cloud and precipitation processes are also of scientific interest, and remote-sensing instruments including radars are a key component of the NSA instrument suite.

One of the radars at NSA is the X-band Scanning ARM Precipitation Radar (XSAPR). This report evaluates one year of recent XSAPR data from April 2024 through April 2025 and details the process of generating b1-level data. This analysis marks the first effort by ARM staff to quality-control NSA XSAPR data with the goal of routinely producing b1-level data in the future depending on radar operations.

1.1 XSAPR Specifications and Scan Strategy

The NSA XSAPR is located atop the Barrow Arctic Research Center (BARC), about 2 km west of the central facility in Utqiaġvik (Figure 1).

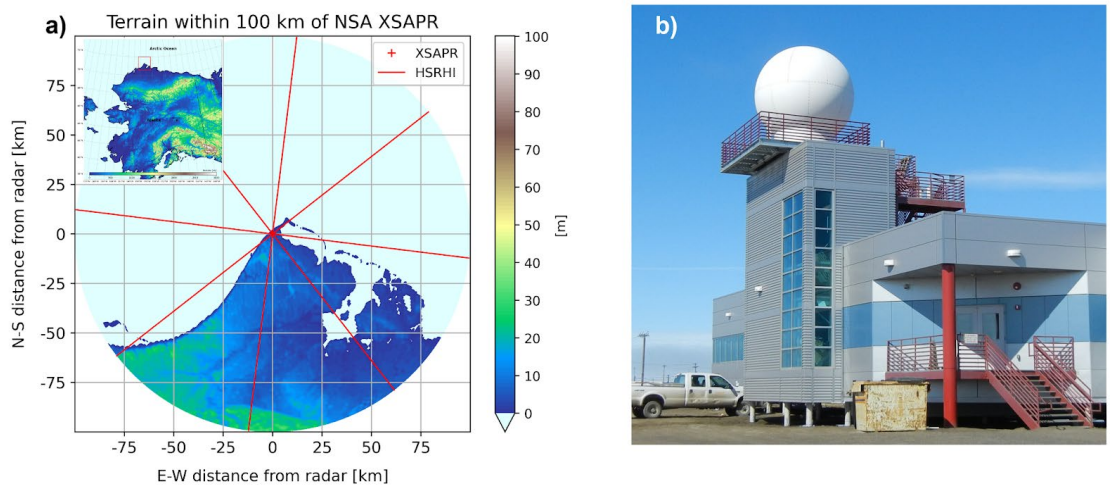

Figure 1. a) Terrain (shaded; m) within 100 km of the NSA XSAPR. A zoomed-out terrain map of Alaska with the radar domain shown in the red square is included in the upper left corner and hemispheric range height indicator (HSRHI) azimuth angles are shown in red. b) the NSA XSAPR installed on top of the Barrow Arctic Research Center (BARC). Image is from the ARM flickr page: https://www.flickr.com/photos/armgov/albums/.

The radar was first installed in 2011 and has been operating intermittently over the last 14 years, with more consistent, recent operations starting in April 2024. As the name suggests, the XSAPR operates in the X-band frequency at 9.67 GHz. The system is dual-polarization, so along with the standard moments

of reflectivity, mean Doppler velocity, and spectral width, parameters including differential reflectivity (ZDR), copolar correlation coefficient (ρ_{hv}), and differential phase are also computed. The XSAPR currently has a range of 100 km when performing plan position indicators (PPIs) with 100-m gate spacing. Additional radar specifications can be found in Table 1.

Table 1. Specifications of the NSA XSAPR.

NSA XSAPR Specifications	
Frequency (GHz)	9.67
Wavelength (cm)	3.1
Transmitter type	Magnetron
Transmit power (kW)	200
Polarization	dual-polarization; simultaneous H and V
Antenna diameter (m)	2.4
3 dB beam width (deg)	1.0
Gate spacing (m)	100
Nyquist velocity (m s^{-1})	10.7

The current XSAPR scan strategy is a mix of PPIs, HSRHIs, and vertically pointing scans (VPTs) that repeat every 15 minutes. The heartbeat begins with four HSRHIs evenly spaced across the domain, including one over the central facility at 97° azimuth (Figure 1a). There are then nine PPIs that are split into two files. The first three are low-elevation scans that can be used to monitor sea ice (-0.5°, 0.0°, and 1.0° elevation). The remaining six are higher elevations ranging from 4.0° to 20.0° (Figure 2). The heartbeat concludes with a VPT that fully rotates once in azimuth, lasting about three minutes.

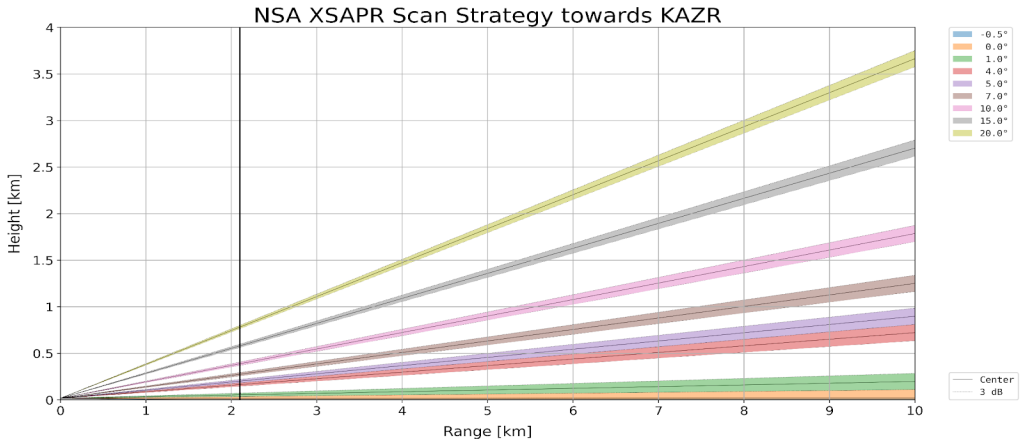

Figure 2. Plot of NSA XSAPR PPI elevation angles as a function of height and distance from the XSAPR (km). The central facility (vertical black line) is located just over 2 km east of the XSAPR. Note that over the central facility, the highest XSAPR PPI elevation angle (20°) is below 1 km.

1.2 Radar Performance

Figure 3 shows the percentage of data files available from the XSAPR based on the current scan strategy. The XSAPR first began collecting data on 12 April, 2024. There were a few prolonged periods between April and November 2024 when the XSAPR was offline, mostly due to various software errors. In early November, an issue with the transmitter air flow sensor was detected and the radar was turned off. The air flow sensor was replaced at the end of November and the radar was operational through most of January 2025 until another, more serious, transmitter problem arose. The XSAPR was offline from 20 January until the transmitter was replaced on 18 March, 2025.

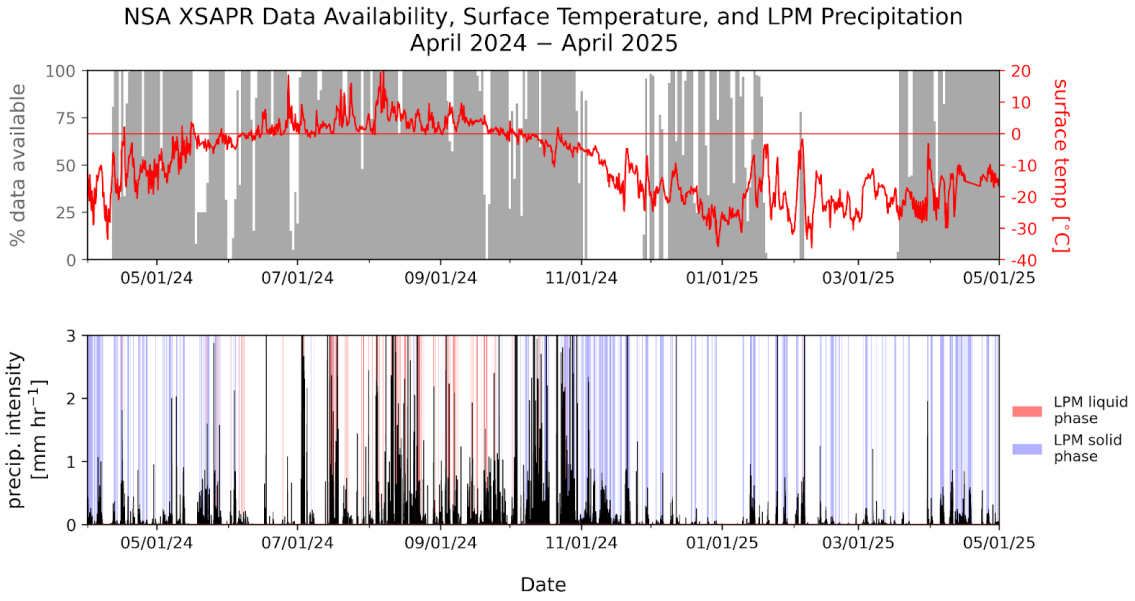

Figure 3. Top: Time series of NSA XSAPR data availability (%; grey bars) and surface temperature from the ARM meteorological station at the central facility (°C; red). Bottom: Precipitation intensity (mm hr^{-1}; black) and hydrometeor phase (red = liquid; blue = solid) from the shielded laser precipitation monitor (LPM) at the central site. Data shown are from April 2024 through April 2025.

Surface temperature from the meteorological station and precipitation rate and phase from the shielded laser precipitation monitor (LPM) at the central facility are also shown in Figure 3 to highlight the frequency of precipitation and the limited period in summer when the temperature is above freezing. This will be important in later discussions of XSAPR reflectivity corrections.

1.3 Outline for b1 Processing

As part of the b-level data processing, a-level data are extensively analyzed and various methods are applied to evaluate key radar parameters including reflectivity and ZDR. The b-level data have corrections applied to these parameters as well as a basic censor mask that distinguishes background noise from signal. Additional data quality issues to note are included in Section 4, some of which are addressed in the b-level data as well.

2.0 Corrections

Various well-established techniques are employed to correct the NSA XSAPR data. The sections below detail the methods used for reflectivity, ZDR, and mean Doppler velocity corrections that are included in the b-level data.

2.1 Attenuation

Attenuation due to atmospheric water vapor and/or hydrometeors can lead to a significant decrease in the power returned to the radar. To evaluate the impacts of gas attenuation on the NSA XSAPR data, PPIs from the XSAPR are matched in time to the nearest sounding launched from the central facility. Gas attenuation is calculated and the maximum is recorded as a function of time and plotted in Figure 4. The maximum gas attenuation within a volume scan occurs in the lowest levels and at the farthest range. Gas attenuation is strongest in the warmer summer months and can be at least 2 dB.

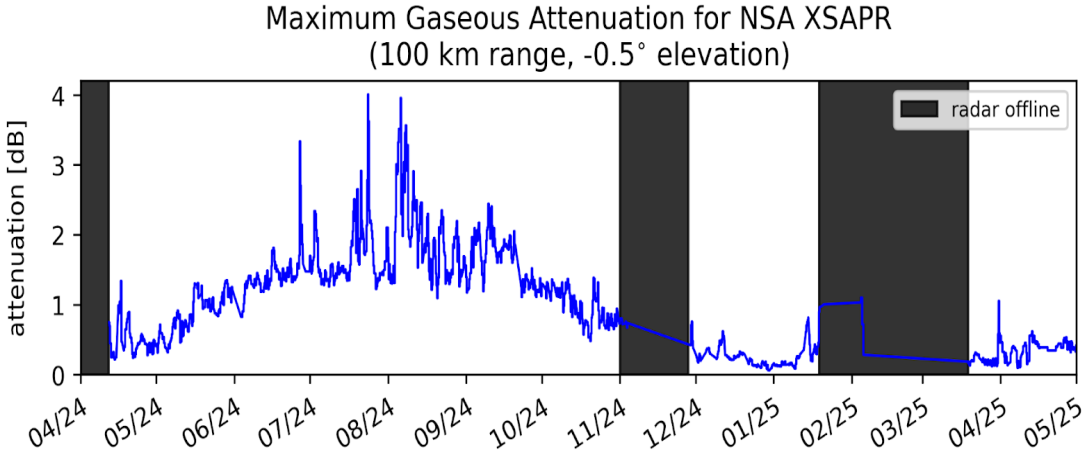

Figure 4. Time series of maximum gaseous attenuation for the NSA XSAPR calculated from soundings launched at the central facility. The maximum attenuation is found at the lowest PPI elevation (-0.5°) and the farthest range (100 km).

Two examples shown in Figure 5 highlight the impact of the local environment on gas attenuation. While both sounding profiles appear saturated, the resulting attenuation is significantly different between the August and October cases due to the temperature differences resulting in different specific humidities. The b-level data does not correct for gaseous attenuation, so additional reflectivity uncertainty at farther range may need to be considered.

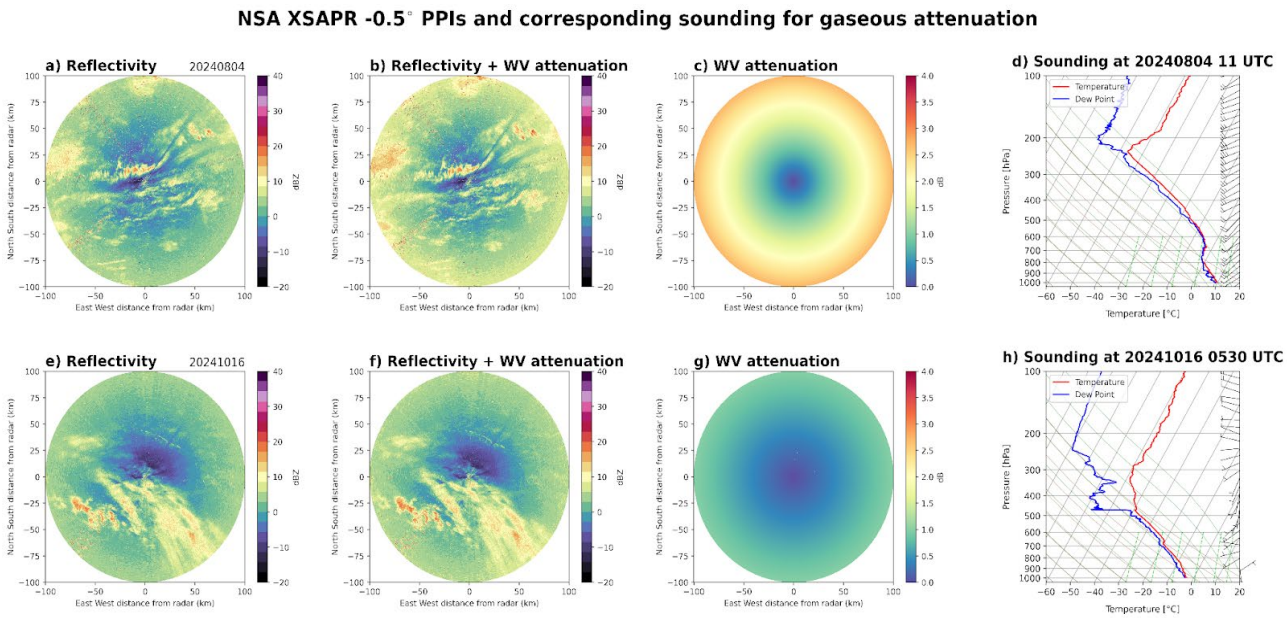

Figure 5. PPIs from the NSA XSAPR at -0.5° of a) reflectivity (dBZ), b) reflectivity with gaseous (water vapor; wv) attenuation applied (dBZ), and c) gas attenuation (dB) on 4 August, 2024 at 11 UTC. d) The corresponding NSA sounding launched from the central facility used to calculate gas attenuation plotted on a skew-T log-p diagram with temperature in red (°C), dewpoint in blue (°C), and wind barbs on the right axis (m s^{-1}). (e-h) as in (a-d) but for 16 October, 2024 at 0530 UTC.

Attenuation from liquid hydrometeors can also decrease the power returned to the radar, especially at X-band. To estimate attenuation from a few rain cases, radar estimates were calculated from the LPM using the PyDSD package (Hardin and Guy 2017). An example of the attenuation calculated from the LPM for a persistent rain event on 15 July, 2024 is shown in Figure 6. The attenuation matches closely with the measured rain rate but rarely exceeds 0.02 dB km^{-1}. Evaluation of the differential phase can also indicate regions of higher attenuation. A PPI of the differential phase for this case at the time of maximum rain rate (16 UTC) is shown in Figure 7 and there are no strong gradients observed. Other rain cases were analyzed with similar results. Given the paucity of rain cases during this correction time period and the lack of gradients in differential phase, the b-level data does not have a hydrometeor attenuation correction applied.

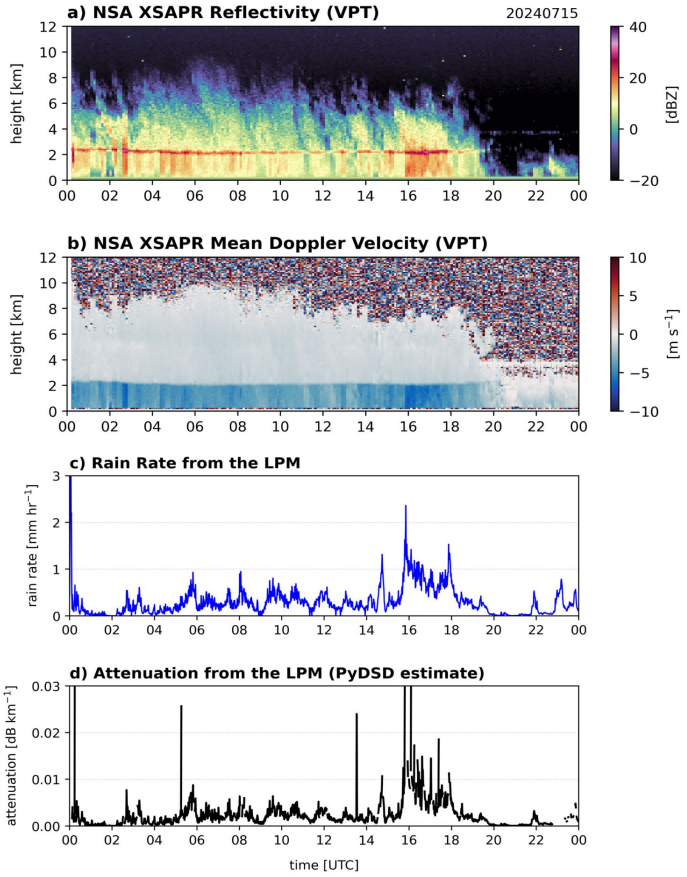

Figure 6. a) Time-height plot of NSA XSAPR reflectivity (dBZ) from the VPT scans on 15 July, 2024. b) As in a) but showing mean Doppler velocity (m s^{-1}). c) Time series of rain rate measured by the LPM (mm hr^{-1}). d) Time series of the attenuation estimated from the LPM calculated using the PyDSD package (dB km^{-1}).

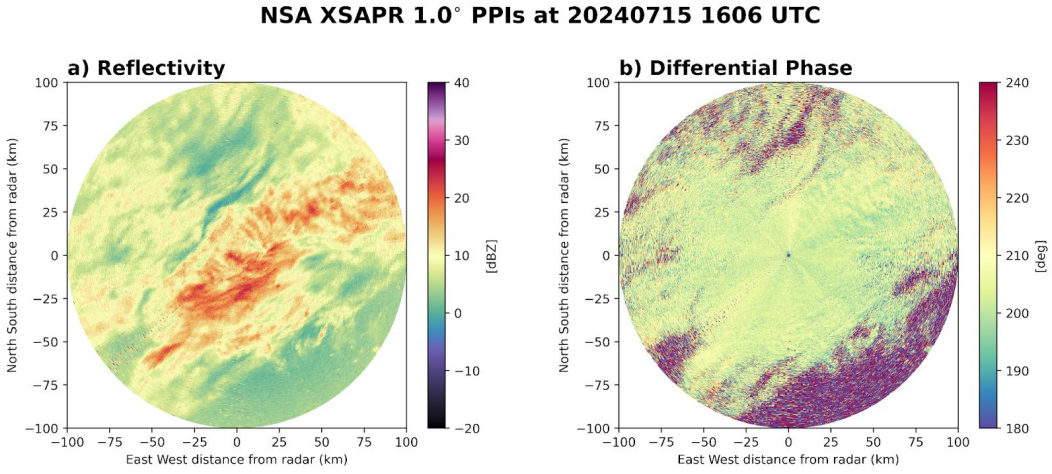

Figure 7. PPIs from the NSA XSAPR at 1.0° of a) reflectivity (dBZ) and b) differential phase (°) on 15 July, 2024 at 1606 UTC.

2.2 Reflectivity

2.2.1 Ground Clutter Stability

To evaluate the stability of the radar hardware, the power reflected by ground clutter targets can be monitored over time. Any significant deviations in ground clutter power may indicate a potential issue with the transmitter. At NSA, clutter is prevalent both over land and over the ocean, particularly at the low-elevation scans (-0.5°, 0.0°, and 1.0°). Clutter targets seen by the XSAPR tend to have higher total power and near 0 m s^{-1} mean Doppler velocity over land. In contrast, sea and ice clutter can have a velocity component and tend to vary more frequently over time. Thus, only stationary targets between 125° and 235° azimuth and within 10 km of the radar (over land) are included in the stability analysis (Figure 8). The daily 95th percentile and mean total power from these clutter points are plotted over time (Figure 9). There are no significant jumps in the values, suggesting the radar is relatively stable, with the 95th percentile being more the consistent of the two metrics.

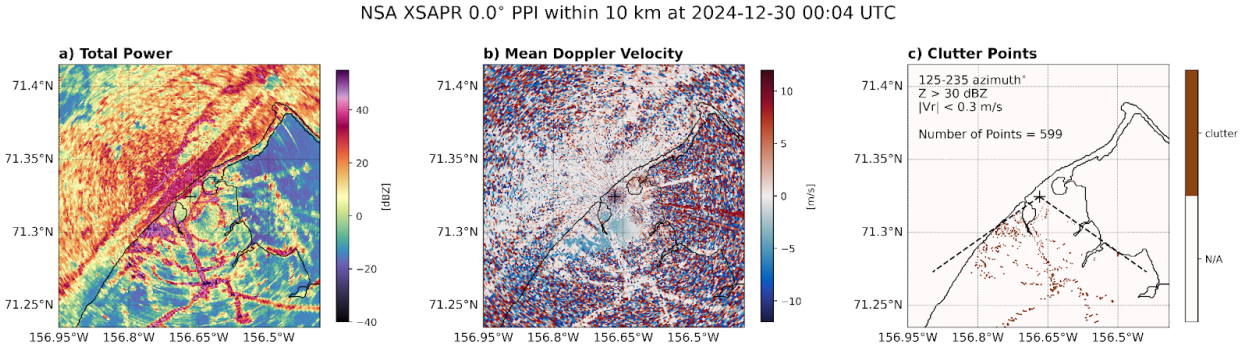

Figure 8. NSA XSAPR PPIs at 0.0° elevation on 30 December, 2024 at 00:04 UTC depicting a) total power (dBZ), b) mean Doppler velocity (m s^{-1}), and c) clutter points detected using set thresholds. All plots are zoomed in to within 10 km of the radar and the Alaska coastline is shown in black.

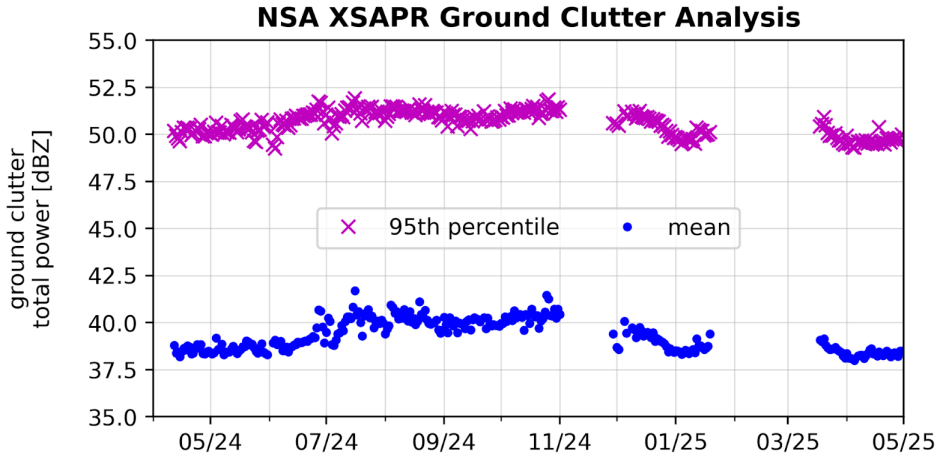

Figure 9. Time series of daily 95th percentile (magenta cross) and mean (blue dot) total power from ground clutter targets from April 2024 through April 2025.

2.2.2 Cross-Comparison with KAZR

NSA XSAPR reflectivity corrections are challenging because of the lack of additional instruments, the lack of auxiliary data from the radar itself, and the paucity of warm rain days. Towards the end of 2025, ARM staff released five years (2020-2024) of quality-controlled b-level NSA Ka-band ARM Zenith Radar (KAZR) data that included corrections to reflectivity based on comparisons with the co-located LPM during the summer months (Rocque et al. 2025). This same comparison method with the LPM was first tested to evaluate the NSA XSAPR reflectivity offsets. Given that the XSAPR is not collocated with the LPM, the PPI and HSRHI data had to be used to extract profiles over the LPM. However, the XSAPR profiles at low levels are significantly contaminated by strong ground clutter, thus rendering this comparison method ineffective. Instead, it was decided that the KAZR would be the reference instrument for correcting XSAPR reflectivity. All KAZR data in this analysis are from the general sensitivity (GE) mode and are already corrected based on the LPM comparisons.

Using HSRHIs from XSAPR over the KAZR site, profiles of XSAPR data can be extracted over the KAZR every 15 minutes. The KAZR data are interpolated in height to match the XSAPR resolution. A case example of this comparison is shown in Figure 10 for 15 May, 2024. For this case, the XSAPR is significantly lower than the KAZR (nearly 9 dB).

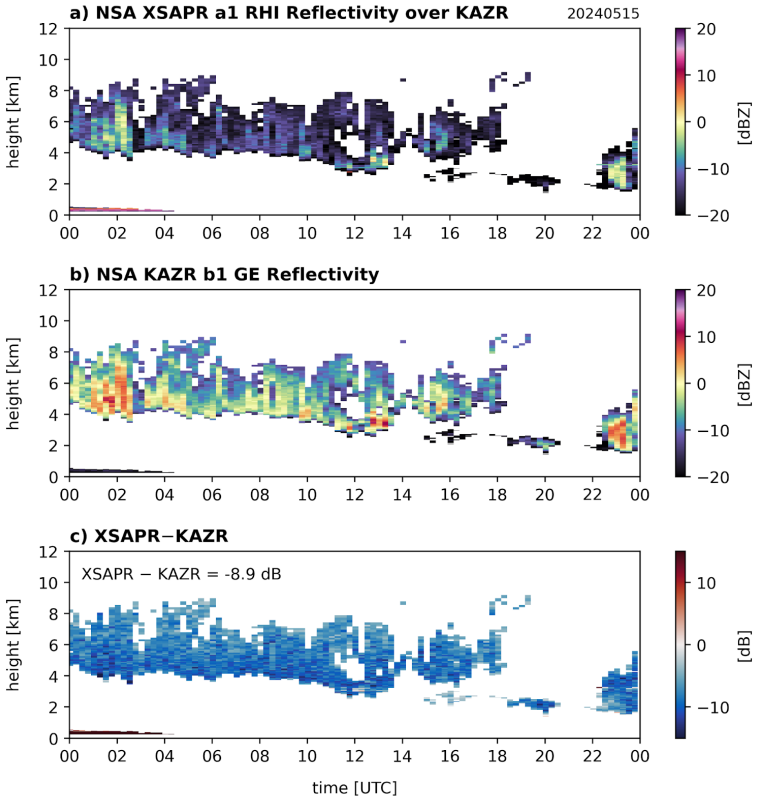

Figure 10. Time-height plots from 15 May, 2024 of a) reflectivity from the NSA XSAPR RHIs over KAZR (dBZ), b) reflectivity from the NSA KAZR GE mode interpolated to XSAPR resolution (dBZ), and c) the difference between XSAPR and KAZR reflectivity (dB). The average reflectivity difference above 4 km is shown in the upper left of panel c) (-8.9 dB).

To eliminate any impacts of attenuation as well as artifacts observed in the XSAPR at low levels (likely due to ground clutter and antenna sidelobes), several thresholds are applied to the comparisons. This analysis is conducted in non-precipitating ice clouds above 4 km and a similar analysis was conducted by Falconi et al. (2018) to calibrate an X-band ARM radar deployed during the Biogenic Aerosols-Effects on Clouds and Climate campaign in Finland. The correlation coefficient from the XSAPR is at least 0.9 and to ensure there are no clouds/precipitation in the low levels, the LPM rain rate is essentially 0.0 mm hr^{-1}. Figure 11 shows a two-dimensional histogram of XSAPR versus KAZR reflectivity with these thresholds applied for April 2024 through April 2025. The majority of points fall between -5 and 5 dBZ and the offset between XSAPR and KAZR is -7.3 dB.

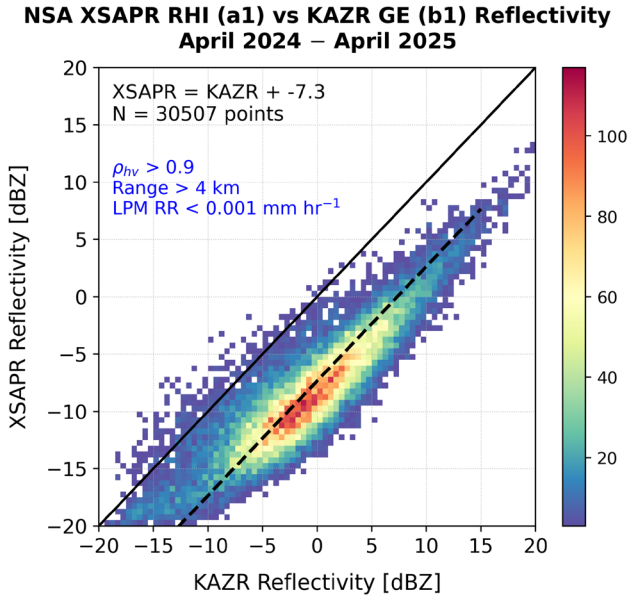

Figure 11. 2D histogram of NSA XSAPR RHI reflectivity versus KAZR GE mode reflectivity for non-precipitating ice clouds aloft where $\rho_{hv} > 0.9$, range > 4 km, and the LPM reports no precipitation. The 1:1 line is shown as the solid black line and the average difference between XSAPR and KAZR when reflectivity is between -15 and 15 dBZ is shown in the upper left corner and as the dashed black line (-7.3 dB).

To make sure there are no significant drifts in the reflectivity offset over time, the daily mean differences between XSAPR and KAZR reflectivity are calculated and plotted in Figure 12. While there are a few outliers observed in July and August 2024, the majority of the daily mean points fall along a mean offset of -7.5 dB. This is in good agreement with the histogram offset in Figure 11. Thus, we conclude that XSAPR is about 7.0-7.5 dB too low.

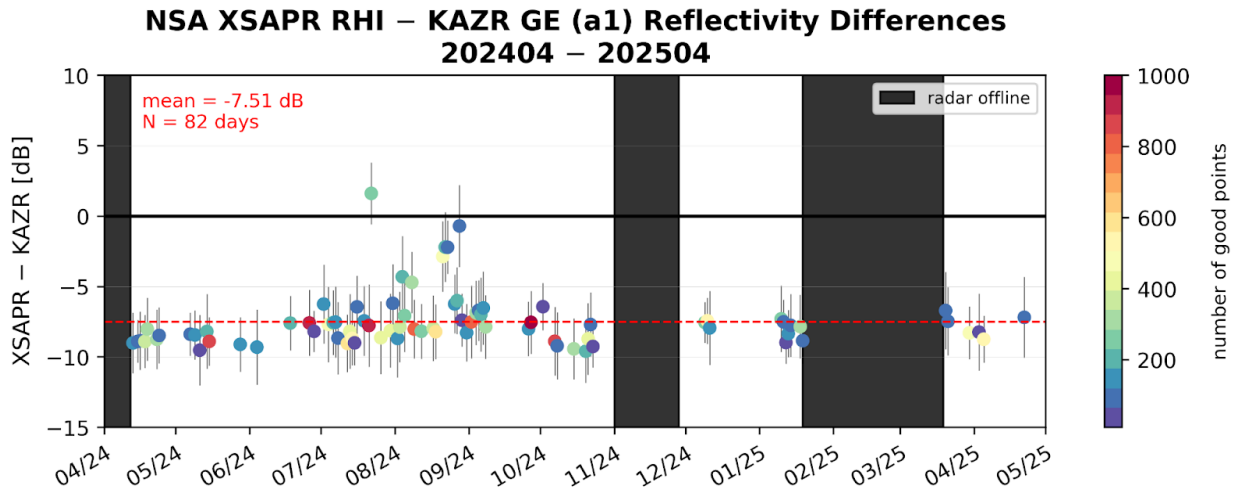

Figure 12. Time series of daily mean reflectivity differences between the NSA XSAPR and NSA KAZR GE mode for April 2024 through April 2025. Days are colored by the number of comparison points and errors bars depict the daily standard deviation. The mean of the daily mean differences is shown in the upper left and as the red dashed line (-7.5 dB).

2.3 Differential Reflectivity (ZDR)

Two methods are used to evaluate the ZDR offset. The first uses VPTs in light rain during the summer months while the second uses PPIs in dry snow during the rest of the year. For the summer method, points are first averaged in azimuth before thresholds are applied to ensure drops are spherical. The thresholds used in this analysis are: reflectivity less than 25 dBZ, signal-to-noise ratio (SNR) greater than 10 dB, ρ_{hv} greater than 0.95, absolute mean Doppler velocity less than 1.5 m s^{-1}, and range between 800 m (above the clutter) and the melting layer (estimated from sounding data). Given the arctic climate, there are not many days when rain is observed at NSA. Thus, another ZDR offset method is tested for winter conditions following the work performed by Colorado State University (CSU) to correct their X-band precipitation radar during the Surface Atmosphere Integrated Field Laboratory (SAIL) field campaign (Chandrasekar et al. 2024). For this method, a winter hydrometeor identification (Thompson et al. 2014) is applied to PPIs at 1° elevation to detect regions of dry snow (ice crystals). Similar thresholds from the summer method are applied here to isolate expected regions of 0 dB ZDR within a 35-km range of the radar.

Daily mean ZDR values from both methods are calculated from the remaining points and plotted as a time series to estimate the ZDR bias and determine any fluctuations over time (Figure 13). Both methods produce similar estimates of the ZDR bias, with an average around -1.5 dB.

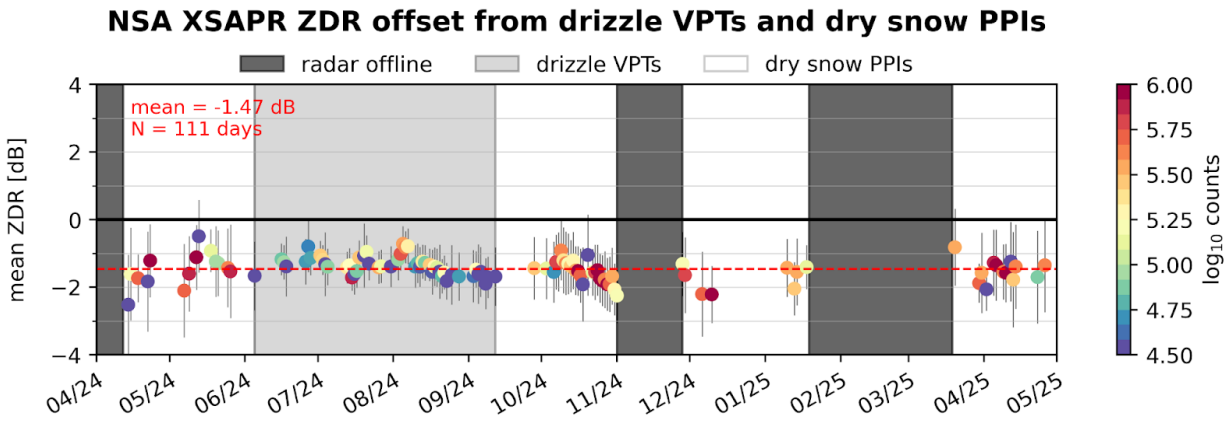

Figure 13. Time series of daily mean ZDR offset from April 2024 through April 2025 calculated using the summer, drizzle VPT method (light grey period) and the winter, dry snow PPI method (white periods). The dark grey periods indicate times when the radar was not operating. The colors of the dots indicate the total number of points per day and standard deviations are shown as error bars. The mean of the daily mean ZDR offset is -1.5 dB across 111 days.

2.4 Mean Doppler Velocity

Prior to 5 September, 2024, the sign of the mean Doppler velocity was backwards. Instead of positive values indicating motion away from the radar, which is the typical convention, the reverse was true. An example of the reversed mean Doppler velocity sign can be seen in Figure 14 displaying VPTs from both XSAPR (incorrect) and KAZR (correct) on 4 August, 2024. The magnitude of the velocity is not impacted, and the sign has been corrected in the b-level data.

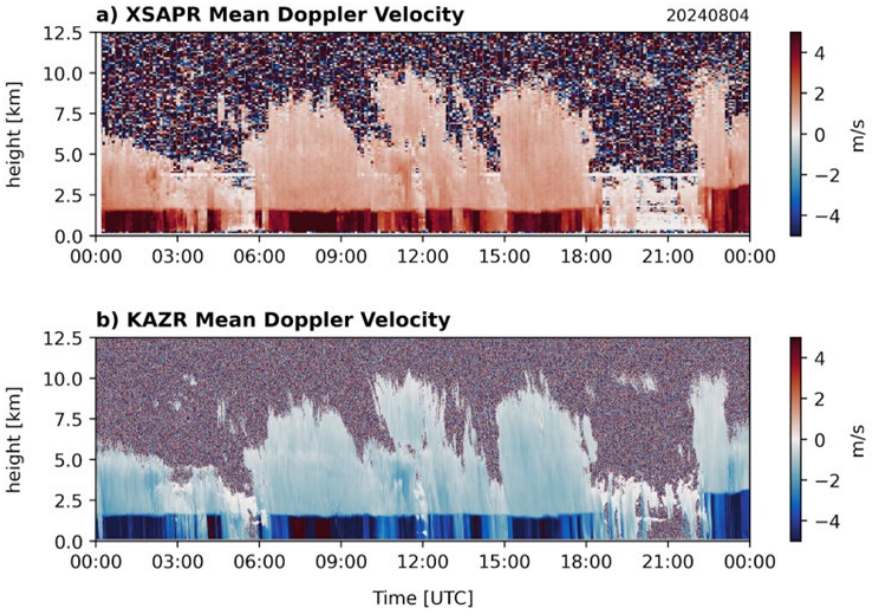

Figure 14. Time-height plots of mean Doppler velocity (m s^{-1}) from a) the XSAPR and b) the KAZR at NSA on 4 August, 2024.

3.0 Mask and Data Examples

As is typical for ARM radar b1 data sets, an echo mask was developed for the NSA XSAPR. This mask is meant to be used as an initial pass at isolating meteorological signals but does not account for clutter that is prevalent within 15-20 km of the site. Users interested in a more refined mask that includes ground clutter, sea clutter, sea ice, and bulk hydrometeor classifications are encouraged to use the Corrected Moments in Antenna Coordinates (CMAC; Collis et al. 2025) Value-Added Product (VAP) data.

Several combinations of variables with different thresholds were tested to optimize the echo mask. Ultimately it was determined that velocity texture (the variation of mean Doppler velocity along range and azimuth) and normalized coherent power (NCP, also known as signal quality index [SQI]) work best for isolating signals. Areas where the velocity texture is less than 2.5 m s^{-1} and the NCP is greater than 0.3 are considered echo targets. An example of the mask and the resulting reflectivity with the mask applied is shown in Figure 15. The mask was tested on a variety of different cases and precipitation regimes, some of which are shown in Figure 16, including widespread precipitation, isolated cells, and cloud streets.

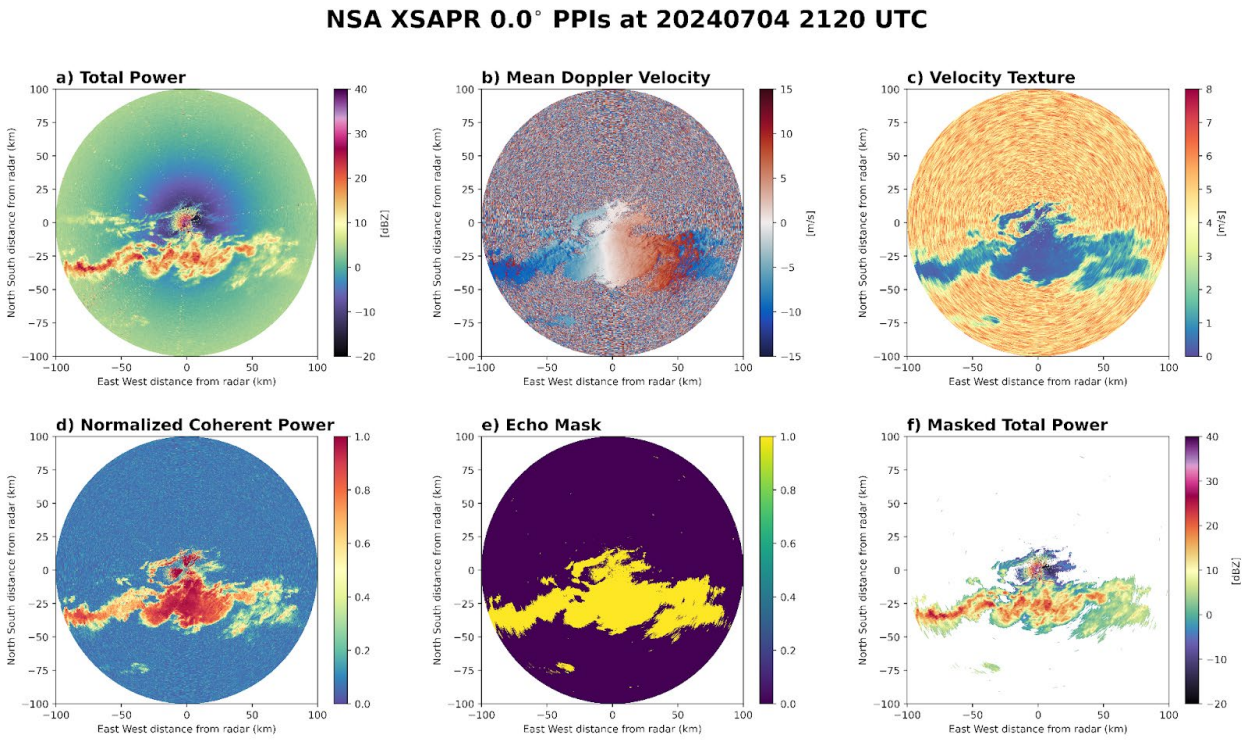

Figure 15. PPIs from the NSA XSAPR at 0.0 on 4 July, 2024 at 2120 UTC. a) Total power (dBZ), b) mean Doppler velocity (m s^{-1}), c) velocity texture (m s^{-1}), d) normalized coherent power (NCP), e) echo mask (yellow = signal), and f) total power with the echo mask applied (dBZ).

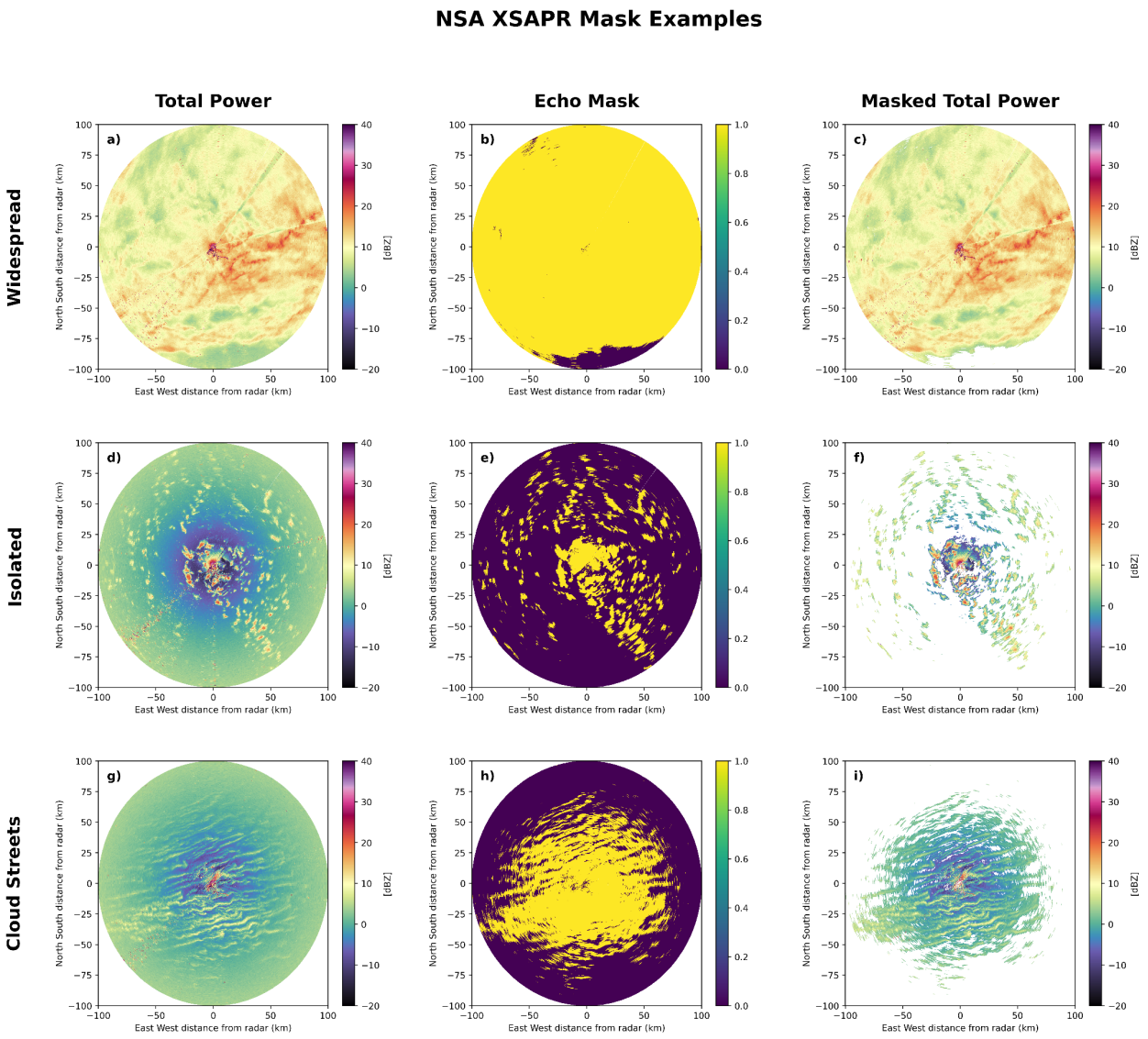

Figure 16. Three cases from the NSA XSAPR highlighting the echo mask in different precipitation regimes: the top panels (a-c) show widespread precipitation, the middle panels (d-f) show isolated cells, and the bottom panels (g-i) show cloud streets. The left panels are total power (dBZ), the middle panels are the echo mask, and the right panels are total power with the mask applied (dBZ).

4.0 Data Quality Issues

4.1 Radial Spikes in Reflectivity and ZDR

Radial spikes in reflectivity and ZDR are frequently observed in PPIs at low elevations. These spikes are not visible in the SNR, the total power (reflectivity without the clutter filter), or when the radar is not transmitting, which suggests they may be related to processing of the data rather than external interference. Figure 17 shows an example of the spikes at 0.0° elevation, which can clearly be seen in the clutter-filtered reflectivity and ZDR fields. Further identification and analysis of the spikes shows they are

most common at the 0.0° and 1.0° elevation sweeps (Figure 18a), they are frequently observed towards the west (over the ocean/ice) rather than to the east (over land; Figure 18b), and they are more often seen in the fall months (September-November; Figure 18c). The spikes influence the magnitude of the reflectivity and ZDR fields in meteorological echoes. The total power can be used instead of the reflectivity, but the ZDR field may be compromised by the spikes so caution should be taken when using this field at low-elevation scans.

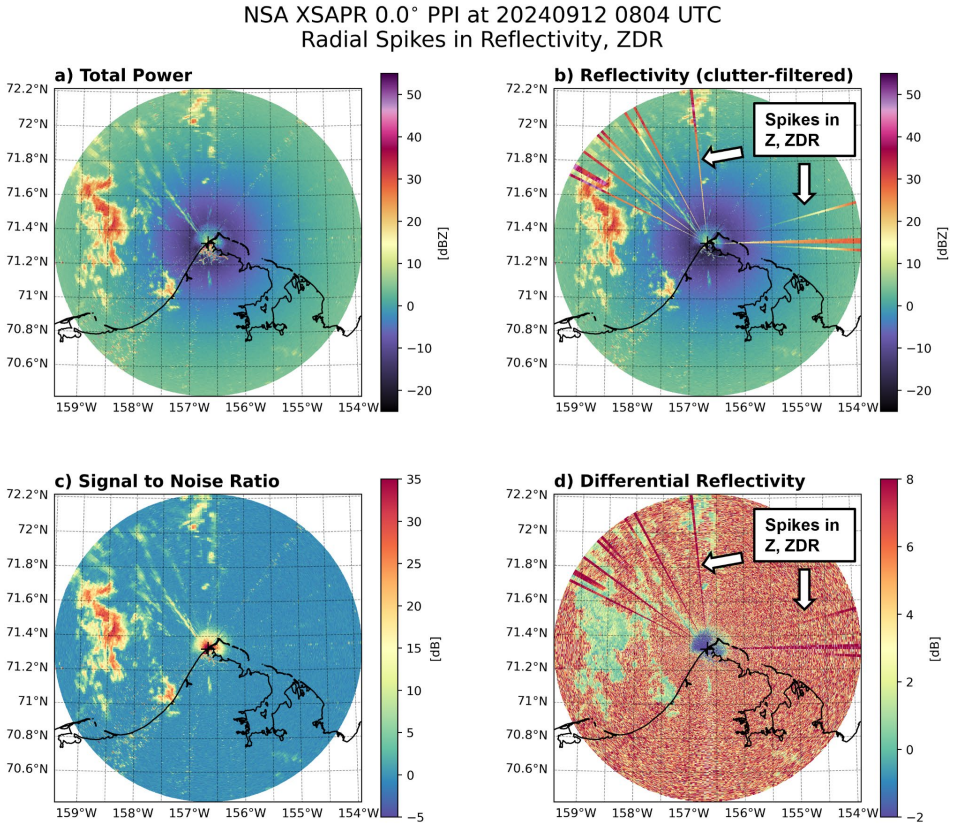

Figure 17. NSA XSAPR PPIs at 0.0° elevation on 12 September, 2024 at 0804 UTC showing a) total power (dBZ), b) clutter-filtered reflectivity (dBZ), c) SNR (dB), and d) ZDR (dB).

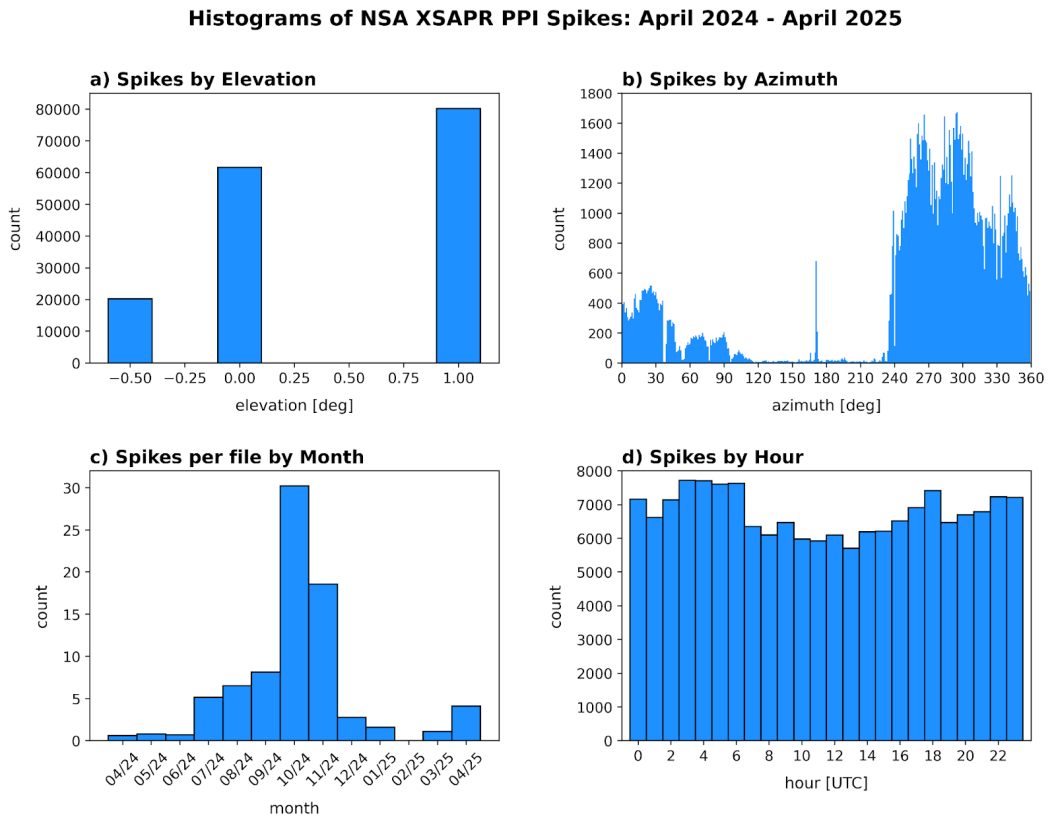

Figure 18. a) Number of NSA XSAPR spikes detected at each low-level PPI elevation angle (-0.5°, 0.0°, 1.0°). b) Number of spikes detected at each azimuth (0°-360°). c) Number of spikes per file detected during each month from April 2024 to April 2025. d) Number of spikes detected during each hour of the day (0-23 UTC).

4.2 Ring of Noise

Following the NSA XSAPR restart at the end of November 2024 after nearly a month of not operating, a "ring of noise" appeared in the data with high SNR. The ring fluctuated in magnitude but remained consistently within three km of the radar. Examples of what this noise feature looks like on a clear day in various types of scans are shown in Figure 19. The noise ring slowly began to weaken over December and was no longer visible in early January 2025. When the ring was most intense in early December, it did appear to impact meteorological echo returns in most of the fields as shown in Figure 20, so data within three km of the radar should be used with caution. While outside of this correction time period, the ring of noise did reappear in June 2025 and the cause is currently under investigation.

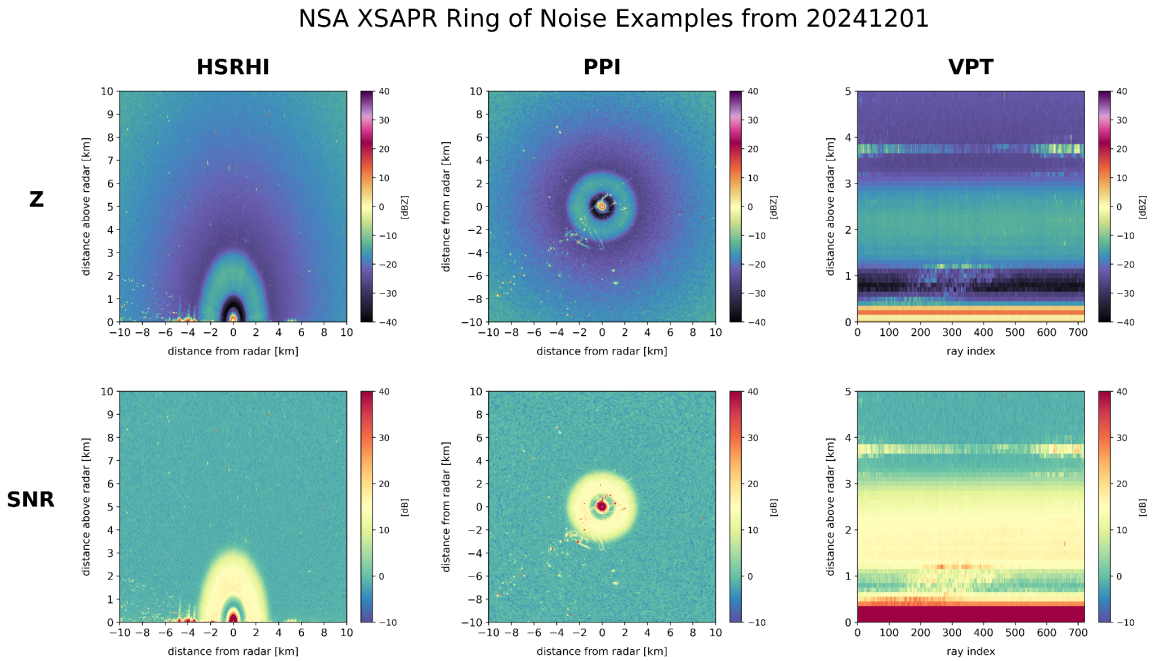

Figure 19. Examples of the ring of noise observed by the NSA XSAPR on 1 December, 2024 around 0530 UTC. Top panels show clutter-filtered reflectivity (Z; dBZ) and bottom panels show SNR (dB). Left panels are from an HSRHI at 97° azimuth, middle panels are from a PPI at 4.0° elevation, and right panels are from a VPT.

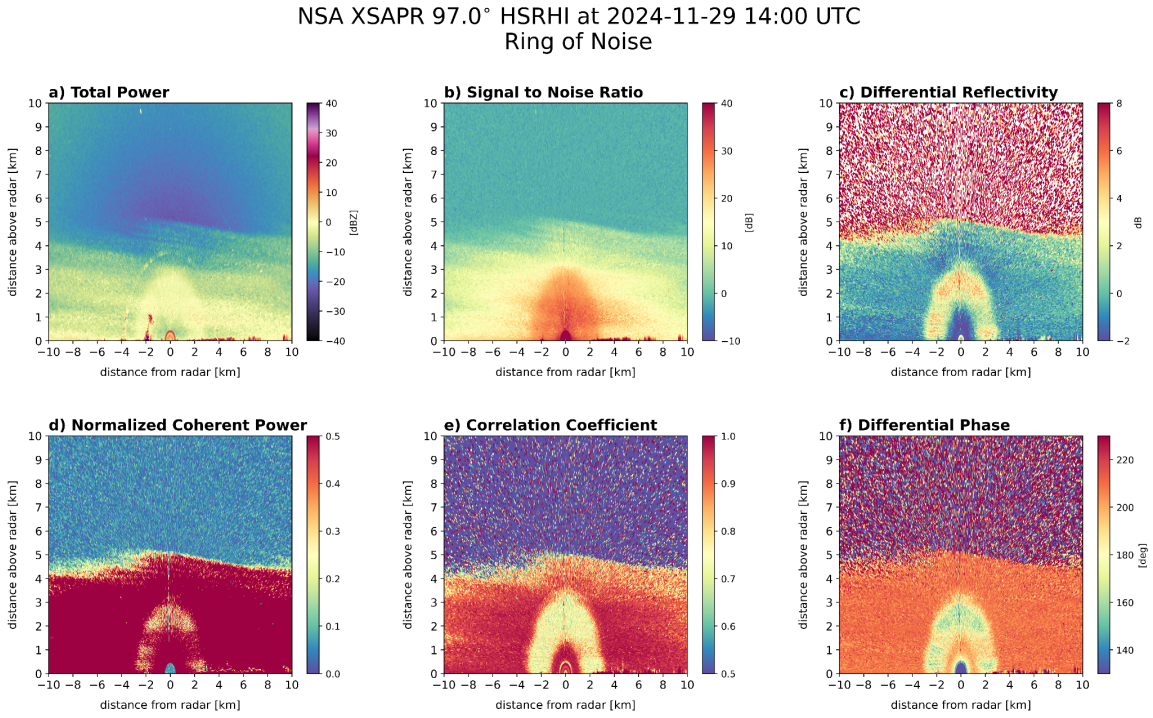

Figure 20. NSA XSAPR HSRHIs at 97° azimuth on 29 November, 2024 at 14 UTC showing a) total power (dBZ), b) SNR (dB), c) ZDR (dB), d) NCP, e) ρ_{hv}, and f) differential phase (°).

4.3 Elevation Jumps at 0.0° and Fixed-Angle Values

When the XSAPR elevation angle is near 0.0°, the values can sometimes jump up to 180° instead of becoming slightly negative. Examples of these jumps in HSRHI and PPI data are shown in Figures 21 and 22, respectively. While not necessarily an issue with the data quality, the jumps in elevation can cause problems with standard plotting methods. These jumps in elevation are fixed in the b1-level data and plots should appear as expected.

In addition to the elevation jumps, the fixed-angle value for the lowest PPI sweep in the a1-level data is 359.5° when it should be -0.5°. This fix has also been applied to the b1-level data.

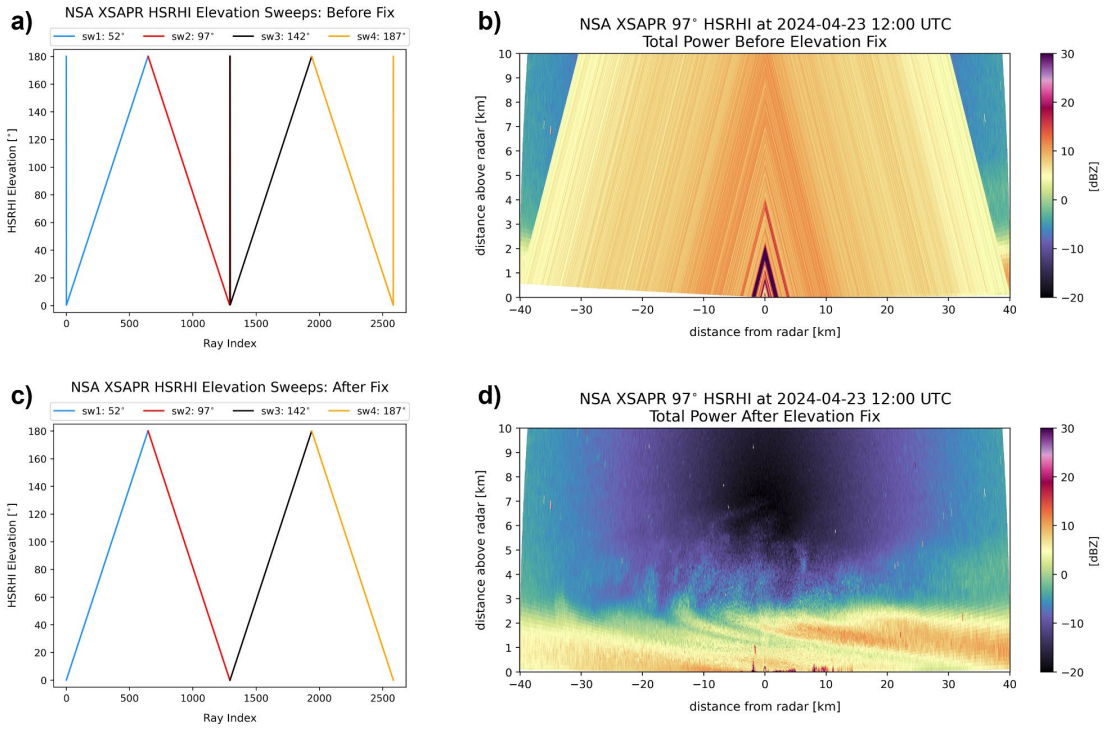

Figure 21. a) NSA XSAPR a1-level HSRHI elevation data colored by each sweep at constant azimuth (blue = 52°, red = 97°, black = 142°, orange = 187°). b) Reflectivity (dBZ) from the NSA XSAPR HSRHI at 97° azimuth. c) As in a) but after the elevation fix has been applied. Note there are no longer sharp increases in elevation from 0° to 180°. d) As in b) but after the elevation fix has been applied. Note the meteorological data is no longer obscured.

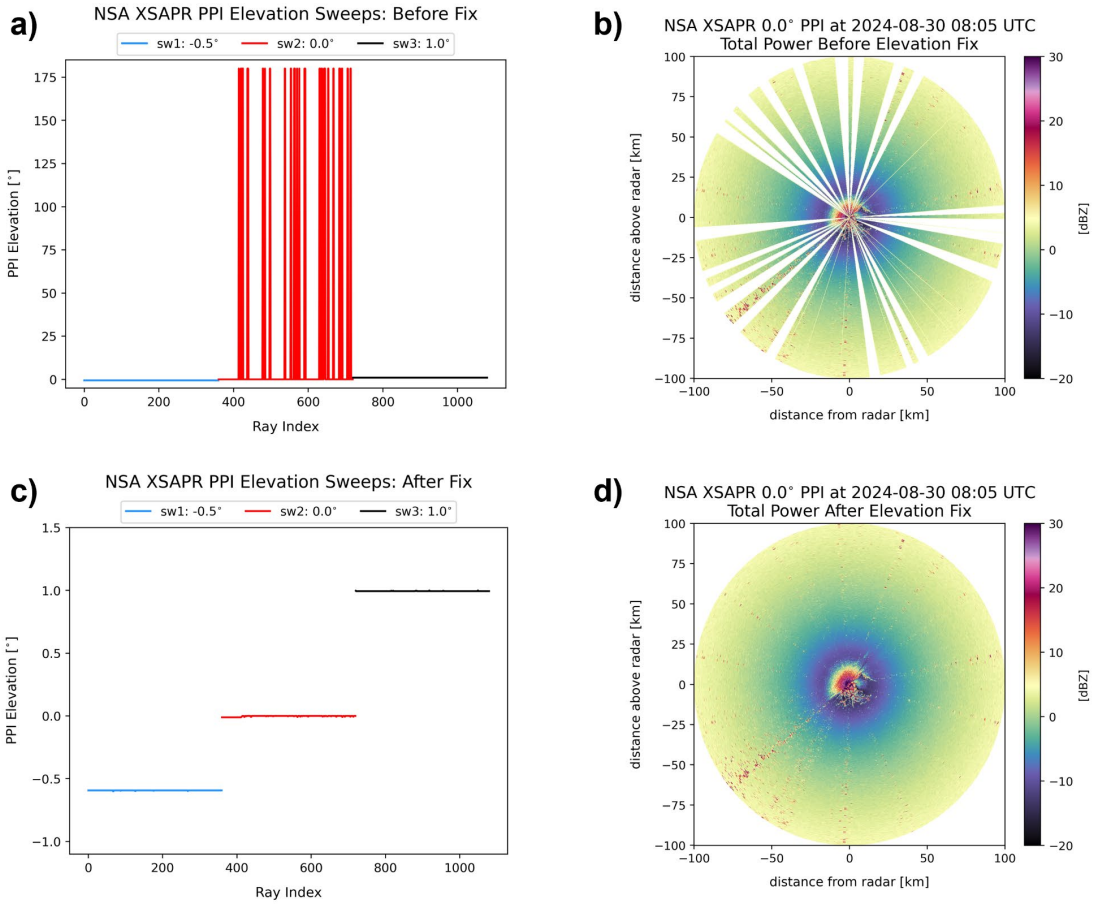

Figure 22. As in Figure 21 but for low-elevation PPIs. Sweeps in panels a) and c) are at -0.5°, 0.0°, and 1.0° and PPIs of reflectivity in panels b) and d) are at 0.0° elevation.

5.0 Description of Data Files

Some of the key variables in the b1-level radar datastream for the NSA XSAPR are listed below. The total power, reflectivity, and ZDR fields have corrections applied and a new censor mask has been developed. Additionally, several variables are left blank as the radar was not reporting these quantities during this time period. These variables are:

- attenuation_corrected_differential_reflectivity
- attenuation_corrected_reflectivity_h
- radar_echo_classification
- reflectivity_enhanced
- reflectivity_v
- total_power_enhanced
- total_power_v

Key
New variable calculated in b1 data
Correction applied

XSAPR File Contents (nsaxsaprcfrqcC1.b1)	
censor_mask	Bit mask 0: no mask 1: horizontal_snr_below_threshold 4: mean_doppler_velocity_texture_above_threshold 8: normalized_coherent_power_below_threshold
cross_correlation_ratio_hv	cross-polar correlation ratio (ρ_{HV})
differential_phase	differential propagation phase shift
differential_reflectivity	differential reflectivity (ZDR) with offset applied
mean_doppler_velocity	radial mean Doppler velocity, positive for motion away from the instrument
normalized_coherent_power	normalized coherent power (NCP), also known as SQI
reflectivity	equivalent reflectivity factor with offset applied
signal_to_noise_ratio	signal-to-noise ratio, horizontal channel
specific_differential_phase	specific differential phase (KDP), calculated by the radar
spectral_width	spectral width
total_power	total power with offset applied, reflectivity without clutter filtering

6.0 References

Chandrasekar, V, F Junyent, and S Biswas. 2024. Calibration and Validation of the SAIL radar.

Collis, S, J Helmus, Z Sherman, R Jackson, B Raut, J O'Brien, M Grover, Y Feng, and A Theisen. 2025. Corrected Moments in Antenna Coordinates (CMAC) Technical Report. U.S. Department of Energy, Atmospheric Radiation Measurement User Facility, Richland, Washington. DOE/SC-ARM-TR-327, https://doi.org/10.2172/3006202

Falconi, MT, A von Lerber, D Ori, FS Marzano, and D Moisseev. 2018. "Snowfall retrieval at X, Ka and W bands: Consistency of backscattering and microphysical properties using BAECC ground-based measurements." *Atmospheric Measurement Techniques* 11(5): 3059–3079, https://doi.org/10.5194/amt-11-3059-2018

Hardin, J, and N Guy. 2017. Software for PyDSD. http://doi.org/10.5281/zenodo.9991

Rocque, M, Y-C Feng, E Schuman, M Deng, A Matthews, and T Wendler. Fixed-Site KAZR b1 Data Processing: Corrections, Calibrations and Processing Report. U.S. Department of Energy, Atmospheric Radiation Measurement User Facility, Richland, Washington. DOE/SC-ARM-TR320, https://doi.org/10.2172/2588592

Thompson, EJ, SA Rutledge, B Dolan, V Chandrasekar, and BL Cheong. 2014. "A dual-polarization radar hydrometeor classification algorithm for winter precipitation." *Journal of Atmospheric and Oceanic Technology* 31(7): 1457-1481, https://doi.org/10.1175/JTECH-D-13-00119.1

www.arm.gov

U.S. DEPARTMENT OF
ENERGY

Office of Science